Gamma-Ray Pulsars

Gottfried Kanbach

Max–Planck–Institut für extraterrestrische Physik, Giessenbachstraße, 85741 Garching, Germany

Abstract. Gamma-ray photons from young pulsars allow the deepest insight into the properties and interactions of high-energy particles with magnetic and photon fields in a pulsar magnetosphere. Measurements with the Compton Gamma-Ray Observatory have led to the detection of nearly ten γ-ray pulsars . Although quite a variety of individual signatures is found for these pulsars, some general characteristics can be summarized: (1) the γ-ray lightcurves of most high-energy pulsars show two major peaks with the pulsed emission covering more than 50% of the rotation, i.e. a wide beam of emission; (2) the γ-ray spectra of pulsars are hard (power law index less than 2), often with a luminosity maximum around 1 GeV. A spectral cutoff above several GeV is found; (3) the spectra vary with rotational phase indicating different sites of emission; and (4) the γ-luminosity scales with the particle flux from the open regions of the magnetosphere (Goldreich-Julian current).

1. Introduction

If the perceptiveness of Jocelyn Bell had not led to the discovery of radio pulsars in 1967, the three brightest localized γ-ray sources would have certainly attracted the attention of the astronomical community. The first high-energy γ-ray maps of the Galaxy (SAS-2, Fichtel et al.,1975; COS-B, Mayer-Hasselwander et al., 1982) are dominated by the sources now known as the young pulsars Crab, Vela and Geminga. Unlike in any other waveband these young pulsars outshine other sources at energies above 100 MeV. The sky survey performed with the Compton Gamma-Ray Observatory (CGRO) from 1991 to 2000 led to the detection of at least 4 more gamma-ray pulsars, raising the total number to 7 sources. Listing also some detections of lower significance we now have about a dozen potential γ-ray pulsars . This is still a small number compared to the known population of radio ($\sim$1500) or X-ray ($\sim$30) pulsars. However the γ-radiation should provide the deepest insights into the physics of the extreme astrophysical site characterized by magnetic fields close to the quantum-mechanical scale

($B_{cr} = m^2c^3/e\hbar = 4.414 \times 10^{13}$ G), space-time near to a fast rotating neutron star, and relativistic speeds in the outer co-rotating magnetosphere. As we will see, the number of detected γ-ray pulsars is quite in agreement with expectations based on sensitivities of current telescopes. Moreover, it is quite likely that several of the unidentified γ-ray sources, which belong mostly to a galactic population and are strongly correlated with population II regions (i.e. molecular clouds, OB associations, SNRs), are γ-ray pulsars without radio emission.

2. High Energy Pulsar Physics

Why can, indeed must, we expect high-energy emissions from young pulsars? Goldreich and Julian (1969) have shown that the magnetosphere of a pulsar is filled with a charge-separated plasma. A rotating, magnetized, conducting neutron star works as a unipolar inductor. The positive and negative charges inside the star, redistributed by the Lorentz forces, arrange themselves such that the electric field from charge separation counterbalances the magnetic forces and no permanent currents flow inside the star. The interior charge distribution determines the electric fields outside the star, requiring continuity for the potentials and tangential electric fields at the stellar surface. The radial components of this magnetospheric electric field ($\sim 6 \times 10^{10} P_s^{-1}$ V cm^{-1}) have a discontinuity on the stellar surface which implies a surface charge layer. The electric fields close to the surface greatly surpass the gravitational attraction as well as the exit work functions of charges from the star. Therefore the magnetosphere of the neutron star is filled with a charge separated plasma which tends to compensate the induced electric fields until $\mathbf{E} \cdot \mathbf{B} = 0$ is achieved and the magnetosphere comes to equilibrium. The required charge density, called the Goldreich–Julian density, is given by

$$n_{GJ} \simeq -\frac{\boldsymbol{\omega} \times \boldsymbol{B}}{2\pi c} = 7 \times 10^{10} B_{\|,12} P_s^{-1} \text{ cm}^{-3}, \quad (1)$$

where $B_{\|,12}$ (units of 10^{12} G) is the field component parallel to $\boldsymbol{\omega}$ and P_s is the rotation period in s.

However there can be no static equilibrium in the co-rotating magnetosphere of a pulsar. At a distance of

$r_c = c/\omega \sim 5 \times 10^4 P_s$ km from the axis of rotation (the 'light cylinder'), particles and fields would have to co-rotate with the speed of light. Relativistic effects of retardation and plasma mass loading will severely distort the pulsar magnetosphere close to the light cylinder and field lines trying to extend across r_c are forced open to the outside. Regions of the magnetosphere threaded by these field lines ('open regions') release their charges into the pulsar wind zone. The outflow leads to a deficit of charges in the regions above the magnetic poles ('polar cap') and between the zero charge density surfaces ($n_{GJ} = 0$) and the equatorial magnetosphere close to r_c ('outer gaps'). In these gaps the electrostatic potential of the rotating dipole is not balanced by charges and is available to accelerate particles to very high energies. Additional accelerating potentials are generated by relativistic effects ('frame dragging') close to the neutron-star surface (Muslimov and Tsygan, 1990, 1992). As a consequence of the described electrodynamics, high-energy particles (Lorentz factors $\sim 10^6 - 10^7$ in most theories, $\sim 10^3$ in some) are accelerated in the gap regions and propagate along the magnetic field. Radiation losses due to magnetic bremsstrahlung (synchro-curvature radiation) and inverse Compton scattering on a low energy photon environment counterbalance the acceleration. If the energies in the particle/photon cascade exceed the threshold for pair creation ($\gamma - \gamma$ and $\gamma - \boldsymbol{B} \rightarrow e^+e^-$), the extent of the acceleration region is further limited by the formation of a dense electron–positron plasma (pair formation front) which screens the open potentials. The high-energy cascade of particles and photons propagates through the magnetosphere until the photons decouple from the particles ('pulsar photosphere') and reach infinity, i.e. our telescopes. The observation of pulsed high-energy radiation allows us therefore to look directly at the particle spectra and magnetic field geometries on the 'pulsar photosphere'. This high-energy photosphere can be visualized as a complex three-dimensional radiating surface with high directivity. Its properties should depend critically on pulsar parameters like field strength, inclination of the magnetic axis, aspect angle of observer, etc. and of course on the model assumptions. Although the scenario of magnetospheric high-energy cascades in the open zones is generally accepted, a fully self-consistent, quantitative theory has not yet been achieved. The terminal energies and spectra reached by the radiating particles depends on many uncertain assumptions and the debate on the relative importance of 'polar cap' and/or 'outer gap' emission continues, with occasional suggestions that the pulsar wind zone could be an additional source of γ-rays . A good set of observational facts, including multi-wavelength spectra and lightcurves, will certainly help to clarify our understanding of these fascinating high-energy machines.

In the following, we qualitatively scale the high-energy radiation output with the current of relativistic particles flowing from the polar cap ('PC'). The Goldreich–Julian
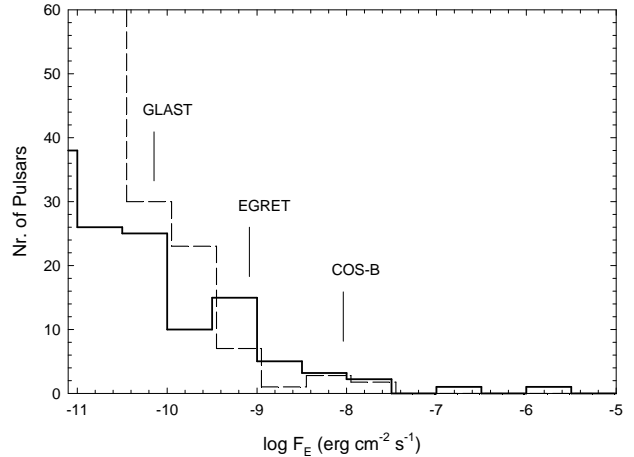

Fig. 1. Distribution of F_E for radio pulsars. For the γ-ray efficiency η two assumptions are used: $\eta = \text{const} = 0.01$(*solid line*) and $\eta \dot{E}_{rot}^\alpha \approx \sqrt{\dot{E}_{rot}}$ (*dashed line*). Approximate sensitivity limits for COS-B, EGRET and GLAST are shown

current, formed by n_{GJ} particles flowing with c from the PC area $A_{PC} \sim \pi r_{NS}^2(\frac{r_{NS}}{r_c})$ is given by

$$\dot{N}_{GJ} = A_{PC} \cdot n_{GJ} \cdot c \sim 1.7 \times 10^{38} \dot{P}^{\frac{1}{2}} P^{-\frac{3}{2}} \text{ s}^{-1}. \quad (2)$$

If this particle flow consists mainly of electrons with Lorentz factor $\sim 10^6$ the outflowing power is of the order of $\sim 10^{38} \dot{P}^{\frac{1}{2}} P^{-\frac{3}{2}}$ erg s^{-1}. It should be noted that the product $\dot{P}^{\frac{1}{2}} P^{-\frac{3}{2}}$ is proportional to $\sqrt{\dot{E}_{rot}}$ and also to the total voltage available over the pulsar's open field lines Φ.

We can now estimate the energy flux observable from a pulsar at distance d:

$$F_E = (\eta \cdot \dot{E}_{rot}^\alpha)/4\pi f_\Omega d^2 \quad (3)$$

where η is an efficiency factor that describes the conversion of the energy input (rotational energy loss or GJ current) into γ-radiation, α an exponent for the energy source (=0.5 if $\dot{N}_{GJ}$ dominates, =1 if $\dot{E}_{rot}$ relates directly to the γ-ray luminosity), and f_Ω describes the solid angle fraction illuminated by the pulsar beam (a canonical value of $f_\Omega = 1/4\pi$, i.e. beaming into 1 sr is assumed). Figure 1 shows the distribution of expected fluxes from a current list of radio pulsars with different assumptions for their luminosities. Rough sensitivity limits for past (COS-B, EGRET) and future (GLAST) telescopes are also shown in fig. 1. COS-B with 4-5 pulsars and EGRET with about a dozen detections are at the expected level. For GLAST we would estimate between 30 and 100 new radio pulsar detections.

These predictions for high-energy emission from radio pulsars were published early after their discovery and the search for pulsars outside the radio range began. Detections were first reported for the Crab pulsar at X-ray (from

balloon-borne detectors) and at optical wavelengths. To-day more than 30 pulsars are known at X-ray energies. In the optical range, four to five pulsating counterparts and a similar number of optical candidates based on positional coincidence have been found.

3. Detections

Table 1 (Kanbach, 2001) gives an overview of the high-energy pulsars and their multi-frequency detections, ranging from the radio band to gamma rays, after the decade of discoveries with the CGRO instruments. Next to the column with the spin period the rank of the quantity $\dot{E}/d^2$, i.e. the spin-down power over the square of the distance as a measure of the apparent brightness, is given. It is evident that the detections in the gamma-ray range follow closely the ranking derived from the spin-down luminosity. Therefore we might conclude that gamma-ray emission is a common phenomenon of pulsars. However, since so far most detections of gamma-ray pulsars require the detection in the radio or X-ray regime in order to provide the periodicity ephemeris, we must be careful not to discard the possibility that many pulsars might exist that emit dominantly at high energies and so far have only been detected as unidentified γ-ray sources.

4. Emission Characteristics

4.1. Lightcurves

The regular brightness variation of pulsars ('lightcurves'), with periods ranging from $\sim ms$ to nearly 10s, was the primary characteristic of this new astrophysical object. The lightcurve of a pulsar can be regarded as the cross-section through a rotating beaming pattern cut along the line of sight to the observer. The full beaming pattern on the sphere around a pulsar would give us a direct view of the sites of origin and beaming directions and allow us to derive the luminosity of such a 'highly' non-isotropic source. But of course we are restricted to our singular view of individual sources. In order to gain a better understanding of high energy pulsars we can follow two routes: (1) rely on theoretical modeling or (2) observe a sufficient number of pulsars to get a statistical relevant sample with different aspect angles. The rather limited number of detections has not yet allowed a full population treatment. But some common traits for the γ-ray emission from young pulsars become already apparent. Figure 2 displays the high-energy lightcurves of the brightest 6 EGRET pulsars. We note that the pulsed emission extends over more than 50% of rotation and sharp peaks (generally 2) limit the 'pulsed' phase interval. The width and dominance of the peaks led to the conventional assumption of a beaming solid angle of 1 sr for luminosity estimates. The likely beaming pattern inferred from these γ-ray lightcurves is in the shape of a cone with high intensity on the rim and lower levels inside ('hollow cone'). Both leading models,
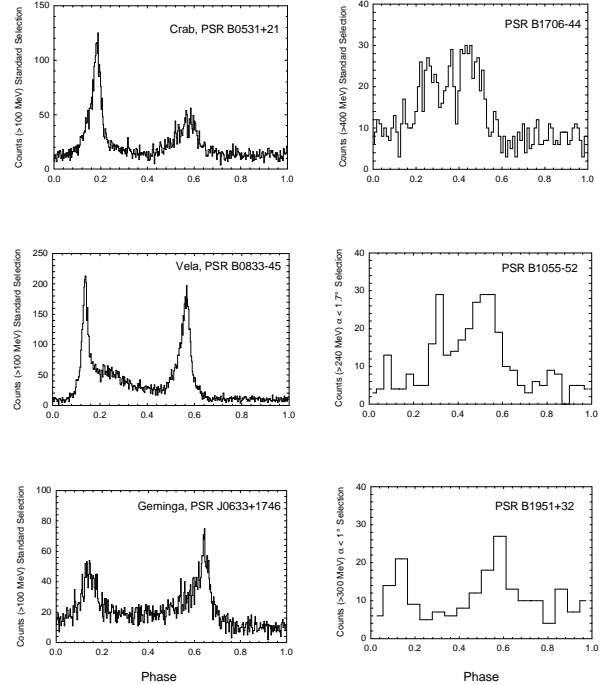

Fig. 2. High-energy light curves of γ-ray pulsars (> 100 MeV, unless indicated differently)

polar cap and outer gap, generate this kind of pattern, although the 2-dimensional shape for the outer gap model could be far from circular. The bright rims of the emission cones indicate the location of intense particle-photon cascades in the magnetospheres. The emission inside the cones is often found to have a harder spectrum, which could indicate that this radiation has been propagated along magnetic field lines with less curvature (polar cap region) avoiding the cascading processes.

In the following we compare the γ-ray lightcurves of the three brightest γ-ray pulsars with their emission at lower energies. These multi-wavelength comparisons serve to distinguish different emission processes. Figure 3 (right panel) shows the Crab pulsar between optical and γ-ray energies. The overall shape of the double-peaked lightcurve remains similar over this range but spectral differences between the components are clearly visible: the bridge region between the two peaks and the second peak are very strong between 100 keV and $\sim$10 MeV. Also in the radio range (left panel figure 3) we find additional structures besides the two peaks: two trailing peaks around 5 GHz and a so-called precursor peak at frequencies below 400 MHz. No comprehensive model has yet been proposed that can explain this complex spatial and spectral emission but it is apparent that several components must exist in the radiation zones of the Crab pulsar.

The same conclusions can be derived for the older pulsars Vela and Geminga. Their multi-wavelength lightcurves are shown in figure 4. Vela is clearly detected

Table 1. High-energy pulsars: multi-wavelength detections, candidates, and positional coincidences
Notes: P: pulsed emission; D: positional coincidence; ?: low significance pulsed detection

PSR	P (ms)	$\dot{E}/d^2$ rank	Radio	Optical	EUV	X_{low}	X_{hi}	γ_{low}	γ_{hi}
High-confidence γ-ray detections									
B0531+21 (Crab)	33.4	1	P	P		P	P	P	P[1]
B0833-45 (Vela)	89.3	2	P	P		P		P	P[3]
J0633+1746 (Geminga)	237.1	3	?	?	P	P		?[9]	P[7]
B1706-44	102.5	4	P			P			P[4]
B1509-58	150.7	5	P	D		P	P	P[2]	
B1951+32	39.5	6	P			P		P[10]	P[5]
B1055-52	197.1	33	P	D		P		P[11]	P[8]
Candidate γ-ray detections									
B0656+14	384.9	18	P	?	D	P		?[10]	?[6]
B0355+54	156.4	36	P			D			?[12]
B0631+10	287.7	53	P						?[13]
B0144+59	196.3	120	P						?[14]
Candidate ms-pulsars γ-ray detections									
J0218+4232	2.32	43	P			P			?[15]
B1821-24	3.05	14	P			P			?[16]
Likely pulsar–γ-ray source coincidences									
B1046-58	123.7	8	P			D			?[18]
J1105-6107	63.2	21	P[17]			D			
B1853+01	267.4	27	P			?			?

References:
[1] Nolan et al.(1993); [2] Matz et al.(1994), Kuiper et al.(1999a); [3] Kanbach et al.(1994);
[4] Thompson et al.(1992, 1996); [5] Ramanamurthy et al.(1995); [6] Ramanamurthy et al.(1996);
[7] Mayer-Hasselwander et al.(1994); [8] Fierro et al.(1993); [9] Kuiper et al.(1996);
[10] Hermsen et al.(1997); [11] Thompson et al.(1999); [12] Thompson et al.(1994);
[13] Zepka et al.(1996); [14] Ulmer et al.(1996); [15] Kuiper et al.(1999b);
[16] Thompson et al.(1997); [17] Kaspi et al.(1997); [18] Kaspi et al.(2000)

as a pulsating source from radio to γ-ray energies. The lightcurves below the γ range are however, in contrast to the Crab case, completely at different phase angles of emission. The same finding applies to the Geminga pulsar. In this case significant pulsed emission has only been detected in the X- and γ-ray region. The present optical and radio detections of Geminga are considered to be of marginal significance and need to be confirmed. We conclude again, that the available multi-wavelength lightcurves show that the magnetospheres of young pulsars contain several additional emitting regions with different spectral and beaming characteristics on top of a basic two-peaked structure.

4.2. Spectra

Thompson et al., 1999 have compiled multi-wavelength spectra for the pulsed emission of γ-ray pulsars as shown in figure 5. The spectral intensities are displayed in terms of νF_ν , which is equivalent to the power emitted per unit interval of $ln(\nu)$. The spectra emphasize that emission in the X- and γ-ray regions dominates the radiation budget of these pulsars and that the pulsed emissions are generally harder than power-laws with index -2 (which would be a horizontal line in this spectral display). In several cases the spectra are curved in the γ-ray range and lead up to a cut-off or turn over at a few GeV. The pulsar spectra are arranged in order of increasing rotational age ($\tau \sim \frac{P}{\dot{P}}$) with Crab ($\tau \sim 10^3 y$) as the youngest and PSR B1055-52 ($\tau \sim 5 \times 10^5 y$) as the oldest object.

The **Crab** pulsar emits the maximum power at about 100 keV and the spectrum can be described by a broad peak extending from the optical band (≈ 1 eV) to about 100 MeV. Above 100 MeV the pulsed spectrum continues with a harder power law distribution up to a few GeV, where the spectrum goes into a steep decline (Kuiper et al., 2001). In addition to the pulsed emission, the Crab shows a strong unpulsed component at high energies. This component has been interpreted to come from the inner Crab nebula as synchrotron radiation below a few GeV and as inverse Compton radiation, up-scattered from optical photons, up to TeV energies.

PSR B1509-58 has been detected in the hard X-ray range by Ginga and at low γ-ray energies up to 30 MeV by BATSE, OSSE and COMPTEL. EGRET may have a marginal detection of this pulsar between 30-70 MeV but
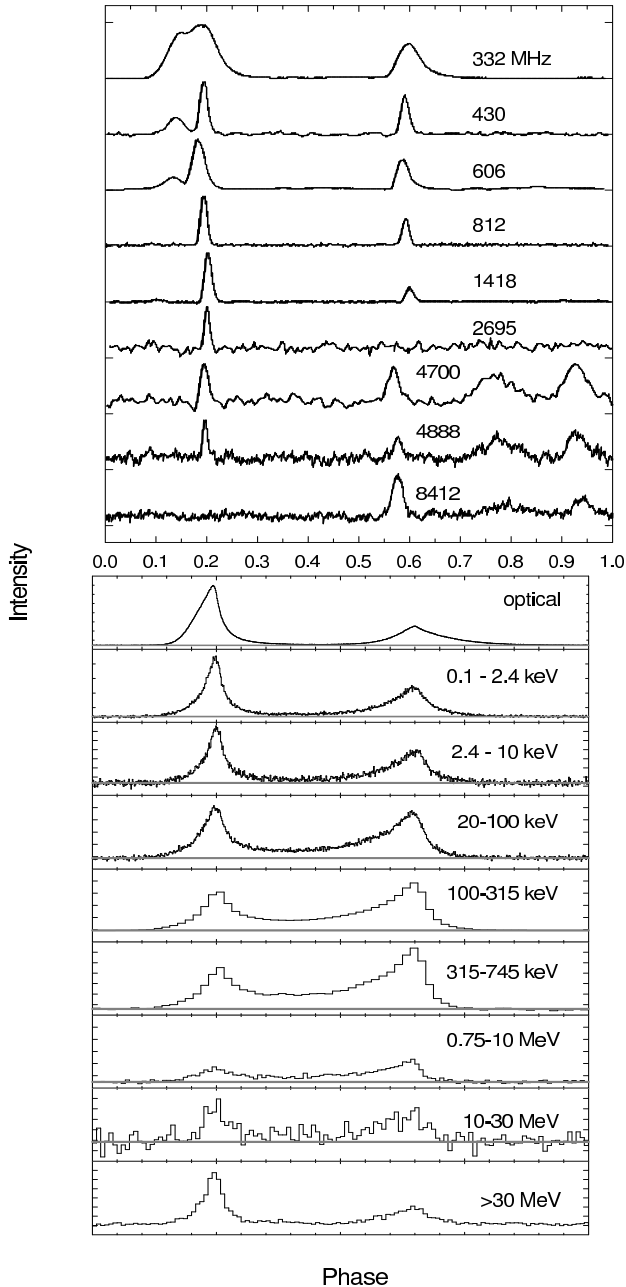
Fig. 3. Multi-wavelength lightcurves of the Crab pulsar in the radio range (top, Moffett & Hankins, 1996) and at high energies (bottom, Kuiper et al., 2001).
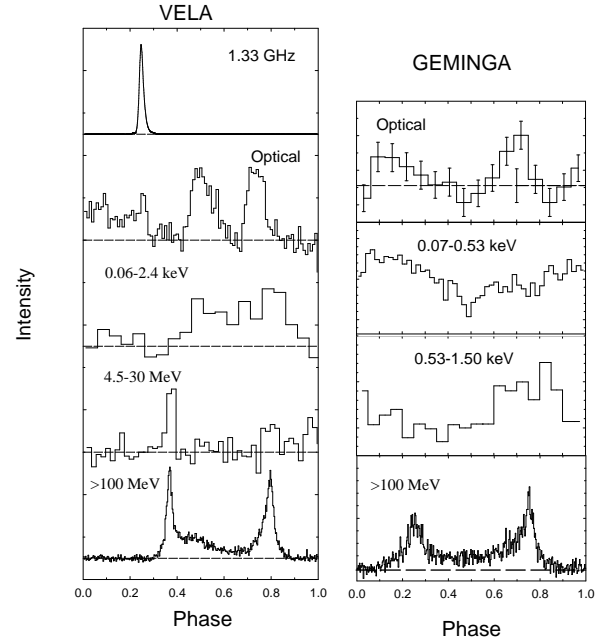
Fig. 4. Multi-wavelength lightcurves of the Vela and Geminga pulsars

elled polar cap photon cascades in such strong fields and find that the second order quantum-mechanical process of 'photon splitting' ($\gamma \to \gamma\gamma$) would limit the energy of emitted γ-rays to several 10's of MeV.

The **Vela** pulsar (PSR B0833-45) has a pronounced spectral break at 2 GeV. Due to the strength of this source, very detailed spectra for the individual phase components, e.g. the peaks and the interpulse emission, are available. The spectra of the emission peaks are generally softer than the spectra of the inter-peak regions. The softest components are observed in the leading and trailing wings of the peaks, which has been explained as a low-energy spill-out from the main γ-ray cascades in the outer magnetosphere.

PSR B1706-44, a γ-ray source that had been detected with COS-B 25 years ago (2CG342-02), was identified in 1992 as a radio pulsar with a 102 ms pulsation period. Although an X-ray source is found coincident with the pulsar no pulsation is found at keV energies. Also at TeV energies the source is detected only as a steady emitter, similar to the Crab. The maximum power of PSR1706-44 is emitted around 1 GeV.

PSR B1951+32 is found as a weak γ-ray source at energies above 300 MeV. After extended EGRET observations, pulsational analysis was successful and confirmed the identification of this γ-ray source with the radio pulsar. The spectrum of this pulsar shows the characteristic spectral break above several GeV only marginally, because of the limited statistics for this source .

Geminga (PSR B0633+17) was the most enigmatic γ-ray source since its detection with SAS-2 in 1972. After long and patient searches with X-ray and optical

places significant upper limits on the flux above this energy range, which indicates that this spectrum must turn over in the ~ 10 MeV range. This low energy spectral cut-off in PSR B1509-58 has been explained as an absorption effect for high-energy photons in the magnetic field. PSR B1509-58 has one of the strongest inferred magnetic fields ($\sim 2 \times 10^{13}$ Gauss, about 40% of B_{crit}) and could be called a 'magnetar'. Harding et al., 1997 have mod-

telescopes Geminga was finally identified as a pulsar in 1992. ROSAT observations revealed a 237 ms pulsations in Geminga (Halpern and Holt, 1972) and the corresponding γ-ray signal was found in data from EGRET, COS-B, and SAS-2. The spectrum of the pulsed emission is generally very hard and shows marked variations over the rotation period. The maximum power of Geminga is emitted at about 1 GeV. Above a few GeV the spectrum breaks off sharply. Geminga is the first specimen of a true high-energy pulsar. The power in optical ($m_v \sim 25.5$, pulsation marginally detected) and radio emissions (marginal detections of pulsed emission at 102 MHz) is lower than the γ-ray emission by more than 6 orders of magnitude, justifying the designation 'radio-quiet pulsar' for Geminga. Speculations that many of the other unidentified galactic γ-ray sources, which appear with comparable brightness, are similar 'Geminga-like' pulsars have been discussed widely. One must realize however that Geminga is a very close (~ 160 pc), low-luminosity pulsar and that the other γ-ray sources, based on their galactic distribution are at least 10 times more distant and therefore should be a hundred times more luminous than Geminga. If the above hypothesis is maintained one has to assume that much younger, high-luminosity pulsars can also operate in a 'Geminga-like' mode. The absence of significant radio- and X-ray counterpart detections for most of the unidentified γ-ray sources requires also that the emission patterns at different wavelengths would not coincide with the γ beams.

PSR B1055-52 also has a very hard energy spectrum that seems to extend from X-rays into the γ-ray range. Again the maximum power is emitted around 1 GeV. No clear break in the spectrum is visible up to 4 GeV. Above that energy a break is required by upper limits at TeV energies.

Figure 6, with an enlarged version of the pulsed spectrum from the Crab, shows the current concept of spectral components in high-energy pulsars. The low energy spectrum, with a peak around 100 keV, is thought to result from synchrotron emission. Based on the spectral maximum of emission from a relativistic electron ($E = \gamma mc^2$) in a magnetic field $B_\perp$ which is at $\nu_{max} \sim 1.2\ MHz \cdot B_\perp(G) \cdot \gamma^2$ an order of magnitude estimate for the peak at 100 keV demands that the product $B_\perp(G) \cdot \gamma^2$ is about 2×10^{13}. Such values could be achieved either with very energetic electrons ($\gamma \sim 10^{6-7}$) in outer magnetospheric fields of ~ 1 Gauss or with electrons of ($\gamma \sim 10^{2-3}$) in inner polar fields with $B_\perp \sim 10^8$ Gauss. The high energy peak could result from inverse Compton scattering of energetic electrons on low energy radiation of energy ε. The typical energy of the inverse Compton photons is then $E_\gamma = \frac{4}{3}\epsilon\gamma^2$, which means that electrons with Lorentz factors $\sim 10^4$ could boost 10 eV photons into the GeV range.

As we saw from the multi-wavelength lightcurves pulsars show spectral changes as they rotate, i.e. the lightcurves look different for adjacent energy bands. This
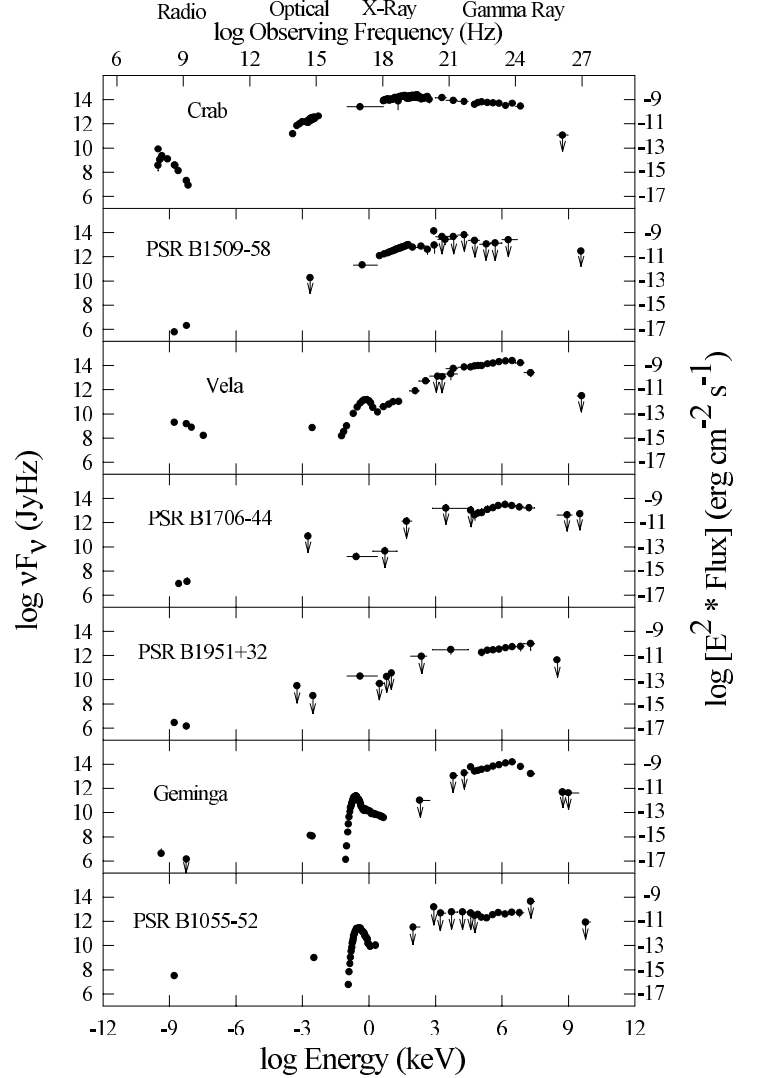

Fig. 5. Multi-wavelength spectra (pulsed emission only) of γ-ray pulsars (Thompson et al., 1999).

phase dependent spectroscopy can be extended to the γ-ray range also. In figure 7 a hardness ratio, defined as the ratio between the number of photons above 300 MeV to those in the band 100-300 MeV, is shown as a function of the pulsar's rotation. We notice that in the prominent '2-peak' pulsars the first peak has a softer spectrum than the interval region. The second peak is generally also harder than the first peak. Model calculations for polar cap cascades (Daugherty and Harding, 1996) as well as the outer-gap model of Romani, 1996 have successfully reproduced these phase-dependent spectra for Vela.

4.3. Luminosities and Energetics

The energy budget of high-energy of pulsars is derived from the pulsed emission spectra by integration from optical wavelengths (~ 1 eV) to the cut-off at GeV energies. The result is given in table 2 where F_E is the observed
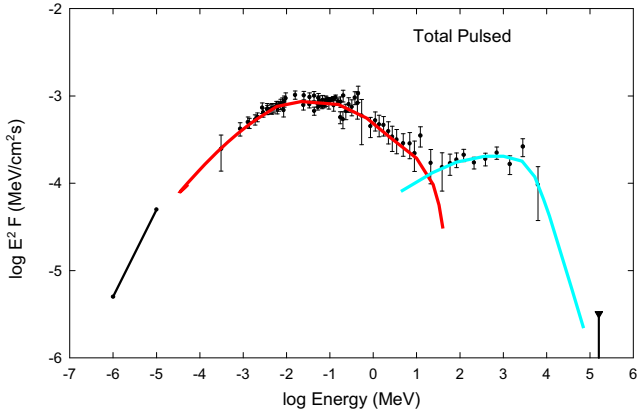
Fig. 6. Pulsed emission from the Crab pulsar with theoretical spectra corresponding to emission via the synchrotron process (low energy peak) and the inverse Compton or curvature radiation peak at higher energies (data from Kuiper et al., 2001).
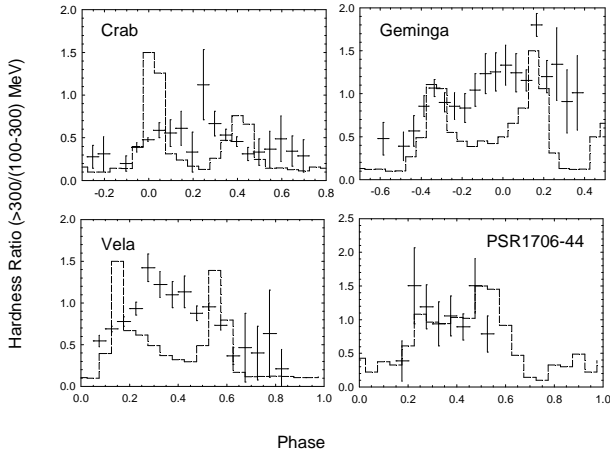

Fig. 7. Spectral hardness as a function of rotation phase for 4 bright γ-ray pulsars . The location of the emission peaks is shown in the underlying lightcurves.

high-energy flux. For the calculation of the efficiency η, with which the pulsar generates energetic photons from the loss of rotational energy, we assume that the emission is beamed into a solid angle of 1 sr. This could be a problematic assumption especially for the wide beaming patterns generated in outer gap models. Figure 8 shows plots of the correlation of the high-energy properties, spectral index and efficiency (≥ 100 MeV) with some derived pulsar parameters: the rotational age ($\tau \propto P/\dot{P}$), the magnetic field ($B \propto \sqrt{P\dot{P}}$) and the total voltage available over the pulsar's open field lines ($\Phi \propto \sqrt{\dot{P}/P^3}$). As many previous investigations have shown, both the efficiencies and the spectral indices for radiation above 100 MeV correlate well with the apparent age and the open field line po-
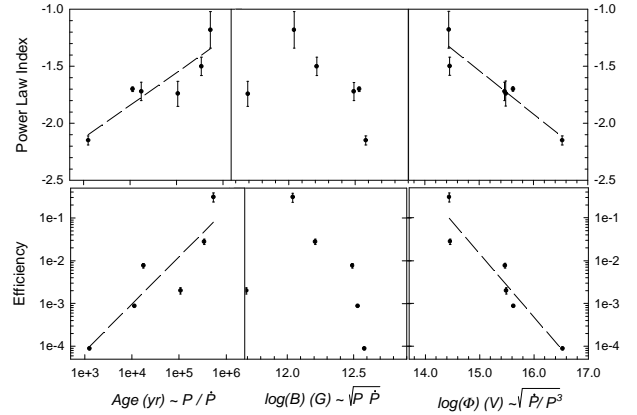

Fig. 8. Correlation of several derived pulsar parameters (rotational age, magnetic field strength, and potential across the polar cap, which is also proportional to the Goldreich-Julian current) with the observed intensity and hardness of γ radiation above $\sim 100 MeV$.
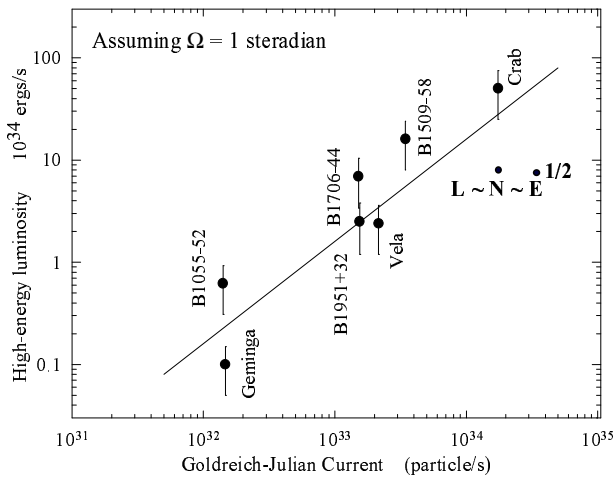
tentials of pulsars. Pulsars become more efficient in their conversion of rotational energy into $E > 100$ MeV radiation and their spectra become harder with increasing age or decreasing potential values. The correlation with the inferred magnetic field is not as clear. Indeed, there seems to be an indication of a decreasing efficiency for both the highest B fields and for low B values. Similarly the spectra appear softer at the marginal magnetic field values. Figure 9 shows directly the correlation between the total high-energy luminosity (≥ 1 eV) and the Goldreich-Julian current. The direct proportionality of $L_\gamma \propto \dot{E}^{0.5}$ is in contrast to the relation at soft X-ray energies $L_X \propto \dot{E}$ (Becker and Trümper, 1997), which could indicate different emission mechanisms in the two bands. As we see in figure 8, the efficiency of some older pulsars appears already quite high ($\sim 20\%$) and a limit tothe conversion of rotational energy into γ-rays must be reached at some value of the open field line potential ($\Phi \leq 10^{14}$ V). Such a condition could indicate the termination of γ-ray production in old pulsars and form a so-called 'death-line' in the conventional $P - \dot{P}$ diagram. Only future, more sensitive, γ-ray observations will be able to define this transition from a 'γ-ray -active' to a 'γ-ray -dead' pulsar more clearly.

5. Conclusions and Outlook

After the mission of the Compton Gamma Ray Observatory we know about a dozen (7 definitely and a few more as likely candidates) γ-ray pulsars. These are objects in which the most extreme electromagnetic and gravitational conditions in the universe act to accelerate highly relativistic particles, leading to high-energy luminosities of the order of 10^{35} erg/s. Young γ-ray pulsars can in principle be observed throughout the Galaxy because γ-rays suffer neither absorption nor dispersion of the pulsed signals.

Table 2. Properties of high-energy pulsars (Thompson et al., 1999)

Name	P (ms)	τ (10^3 yr)	$\dot{E}$ (10^{36} erg s^{-1})	F_E (erg cm^{-2} s^{-1})	d (kpc)	L_{HE} (erg s^{-1})	η ($E > 1$eV)
Crab	33	1.3	450	1.3×10^{-8}	2.0	5.0×10^{35}	0.001
B1509-58	150	1.5	18	8.8×10^{-10}	4.4	1.6×10^{35}	0.009
Vela	89	11	7.0	9.9×10^{-9}	0.5	2.4×10^{34}	0.003
B1706-44	102	17	3.4	1.3×10^{-9}	2.4	6.9×10^{34}	0.020
B1951+32	40	110	3.7	4.3×10^{-10}	2.5	2.5×10^{34}	0.007
Geminga	237	340	0.033	3.9×10^{-9}	0.16	9.6×10^{32}	0.029
B1055-52	197	530	0.030	2.9×10^{-10}	1.5	6.2×10^{33}	0.207

Fig. 9. Pulsar luminosity above ~ 1 eV, assuming a beaming pattern solid angle of 1 sr, versus the Goldreich–Julian current flowing from the open magnetosphere. (Thompson et al., 1999).

High-energy radiation from magnetized rotating neutron stars is not only a fascinating astrophysical topic in itself – a thorough understanding of the radiation processes also opens the way to uncover the true nature of some of the presently unidentified γ-ray sources. The majority of these objects are galactic (their distribution correlates well with the galactic disk) but the ~ 170 objects of the EGRET catalog ($\sim 60\%$ of all γ-ray sources) pose a major challenge and puzzle to astronomy. It is known that the γ-ray sources correlate generally with regions containing young populations like molecular clouds, star forming regions, OB associations, HII regions, or SNRs. We can safely assume that these regions also contain young pulsars that have not yet been revealed, either being hidden inside their birth places or for a lack of emission at other wavelengths. As described above, Geminga can be taken as a rôle model for such a population of pure γ-ray pulsars. The discovery of individual young γ-ray pulsars will certainly support our theoretical understanding of pulsar physics, but their population will also provide us with new insights into active star forming regions and the processes leading to the formation of neutron stars. Overall the contribution

of unresolved, distant pulsars to the diffuse galactic γ-ray emission could be in the range of 5–30%.

The next generation of γ-ray telescopes, especially the GLAST project as a successor to EGRET (Michelson, 1996), will be much more sensitive and is expected to discover 30 - 100 new γ-ray pulsars based on the catalog of radio pulsars alone. With the much higher sensitivity of GLAST and the resulting high photon detection rate it will also be possible to investigate many unidentified γ-ray sources for periodicities independent of observations at other wavelengths. For EGRET this capability for independent periodicity detection has been demonstrated only for Geminga (Brazier and Kanbach, 1996; Chandler et al., 2001). None of the other EGRET sources has a signal/noise ratio with a high photon detection rate similar to Geminga and the powerful investigation for periodicities in some strong EGRET sources carried out by Chandler et al., 2001 was unsuccessful. Thus the next generation of γ-ray telescopes has the potential to reveal the radiation physics of pulsars with a wide range of ages and to discover a new population of pure high-energy pulsars.

References

Becker, W., and Trümper, J., 1997, A& A, **326**, 682
Brazier, K.T.S., and Kanbach, G., 1996, A& A Suppl., **120**, 85
Chandler, A.M., et al.,2001, ApJ, **556**, 59
Daugherty, J.K., and Harding, A.K., 1996, ApJ, **458**, 278
Fichtel, C.E., et al.,1975, ApJ, **198**, 163
Fierro, J.M., et al.: 1993, ApJ, **413**, L27
Goldreich, P., and Julian, W., 1969, ApJ, **157**, 869
Harding, A.K., Baring, M.G., and Gonthier, P.L., 1997, ApJ, **476**, 246
Halpern, J.P., and Holt, S.S., 1992, Nature, **357**, 222
Hermsen, W., et al., 1997, in *The Transparent Universe*, Proc. 2nd INTEGRAL Workshop, St. Malo, France, ESA SP-382, 287
Kanbach, G., 2001, Gamma-Ray Pulsars. In: The Universe in Gamma Rays, (Ed.) V. Schönfelder. Springer Verlag, Berlin, 127
Kanbach, G., et al., 1994, A& A, **289**, 855
Kaspi, et al., 1997, ApJ, **485**, 820
Kaspi, et al., 2000, ApJ, **528**, 445
Kuiper, et al., 1996, NATO-ASI No.515, p.211
Kuiper, L., et al., 1999a, A& A, **351**, 119
Kuiper, L., et al., 1999b, Astrophys.Lett. and Comm., **38**, 33

Kuiper, L., et al., 2001, A& A, **378**, 918

Matz, S.M., et al., 1994, ApJ, **434**, 288

Mayer-Hasselwander, H.A., et al., 1982, A& A, **105**, 164

Mayer-Hasselwander, H.A., et al., 1994, ApJ, **421**, 276

Michelson, P.F., 1996, SPIE, **2806**, 31

Moffett, D.A., and Hankins T.H., 1996, ApJ, **468**, 779

Muslimov A.G. and Tsygan A.I.: 1990, Astron.Zh., **67**, 263

Muslimov A.G. and Tsygan A.I.: 1992, MNRAS, **255**, 61

Nel, H.I., et al., 1996, ApJ, **465**, 898

Nolan, P.L., et al., 1993, ApJ, **409**, 697

Ramanamurthy, P.V., et al., 1995, ApJ, **447**, L109

Ramanamurthy, P.V., et al., 1996, ApJ, **458**, 755

Romani, R.W., 1996, ApJ, **470**, 469

Thompson, D.J., et al., 1992, Nature, **359**, 615

Thompson, D.J., et al., 1994, ApJ, **436**, 229

Thompson, D.J., et al., 1996, ApJ, **465**, 385

Thompson, D.J., et al., 1997 Proc. of the 4th Compton Symp.,
    eds. C.D. Dermer et al., Williamsburg, Va., AIP CP410, 39

Thompson, D.J., et al., 1999, ApJ, **516**, 297

Ulmer, M.P., et al., 1996, ApJ, **448**, 356

Zepka, A., et al., 1996, ApJ, **456**, 305